Phytic acid as a biomass flame retardant for Polyrotaxane based phase change materials

Guang-Zhong Yin, [a, b] Xiao-Mei Yang, [a] José Luis Díaz Palencia,[c] Jose Hobson, [a] Alba Marta López,[a] De-Yi Wang [a, b,] *

[a] *IMDEA Materials Institute, C/Eric Kandel, 2, 28906 Getafe, Madrid, Spain*

[b] *Universidad Francisco de Vitoria, Ctra. Pozuelo-Majadahonda Km 1,800, 28223, Pozuelo de Alarcón, Madrid, Spain*

[c] *Universidad a Distancia de Madrid, Carretera de La Coruña, km 38,500, vía de servicio, 28400, Madrid, Spain*

ABSTRACT. Petrochemical resources are facing depletion and human long-term survival needs sustainable development. In this era, it is very important to develop new sustainable phase change materials (PCMs), because it has shown great application value in the effective utilization of industrial waste heat, solar energy harvesting, and electronic heat treatment. In this work, we reported a biomass phytic acid (PA) modified polyrotaxane (PLR) as PCMs for thermal management. The tensile performances, fire safety, phase transition performances of the PCMs were investigated. It is found that all the tensile properties, char residual, and fire-safety of PLR can be enhanced remarkably by introduce of PA. Typically, the Young's modulus, yielding strength and tensile strength of the PLR were 826.7 MPa, 14.2 MPa and 14.2 MPa, respectively, and significantly increased to 1527.4 MPa, 22.1 MPa, and 24.0 MPa respectively, with the addition of 10 wt.% of PA. Elongation (>783 %) for all modified PCMs was gradually increased with the increase of PA contents. Thermal analysis shows that the fire safety of

1

21   PLR is significantly improved. Specifically, for the best sample PLR-PA30, the pHRR could decrease

22   by 54.2 %, THR decreased by 34.0%; and the LOI increased from 20.8% to 28.2%. The PCMs showed

23   the perfect form stability and leakage-proof performance, enhanced thermal conductivity and

24   outstanding cycle properties. Notably, its biomass source, and high flexibility, enhanced fire safety and

25   completely green pathway may provide a practical way for the highly flexible and sustainable packaging

26   of electronic devices for heat treatment.

27   KEYWORDS: Polyrotaxane, Phase change materials, Phytic acid, Biomass, Shape memory materials

28

1. INTRODUCTION

Bill Gates recently pointed out that climate warming will be a global disaster that may be more extensive, serious and far-reaching than the COVID-19. In order to avoid disaster, reverence and awe of nature is a life attitude everyone should have; low carbon emission and sustainable development need to be the primary concern of material scientists and chemists; and clean energy, green chemistry and environmental protection manufacturing should be our preferred scientific proposition and main direction. Phase change materials (PCMs) have attracted more and more attention recently in the corresponding field of thermal regulation [1, 2] energy saving, harvesting and storage. [3-5] Nowadays, PCMs involving high melting enthalpy have been applied for heat regulation of electronic devices. [6, 7] However, it is still a big challenge to apply PCMs conveniently because of their solid rigidity nature and leakage problem. Considerable strategies have been dedicated to prepare flexible PCMs by blending PCMs substances with some other flexible polymers. [8-10] The design and preparation of intrinsically flexible PCM films are also well explored. [11] With the further development of 5G technology, the amount of PCMs requests for both smart heat regulation and the safety concerns increases. However, the organic PCMs are easily flammable, e.g., PEG and paraffin. The fire safety is still the main limitation for the practical applications of organic PCMs. Thus, it is imperative to improve the fire safety for advanced PCMs.

Nowadays, introducing flame retardants into PCMs is a most widely used pathway to enhance the flame retardancy of PCMs. [12-17] On the other aspect, some renewable resources like DNA, [18, 19] chitosan, [20] soy protein, [21] starch, [22] and phytic acid (PA) [23-25] have been widely applied as sustainable flame retardants in the past decades. PA, an eco-friendly molecule, is biocompatible, biodegradable, nontoxic, and phosphorus-rich (28 wt.%). [26] Thus it has been widely used as a bio-

51 based flame retardant for polymers. [27, 28] For examples, the double coatings (i.e., layer-by-layer self-

52 assembly) by varied combinations of egg white protein and PA were explored to flame retard cotton

53 fabrics. Thermogravimetric analysis (TGA) in air show that the char residues increases up to 32.9 wt.%

54 at 600 °C, which is obviously superior to the results of literature reports with other flame retardants.

55 [24]

56   Polyrotaxane (PLR) is a new type of flexible and intelligent multifunctional PCM. [29] It performed

57 excellent flexibility, mechanical strength and shape memory properties, thermoplastic properties, and

58 easy to be fabricated and functionalized. [30] It has significant practical significance to further develop

59 its applications.[31] As known, PLR is prepared in water. To realize good dispersion, water soluble,

60 eco-friendly flame retardant is a good choice. Furthermore, it is reported the liquid-like modifier can

61 act as an inter-pore bridge for a more homogeneous stress distribution, which ensures high mechanical

62 properties. [32] It is reported that the introduce of multiple hydrogen bonds into polymer system may

63 enhance the mechanical properties. [33-35] Therefore, we will use PA liquid as the flame retardant

64 modifier directly, and use it as acid source to prepare flame retardant PLR based PCMs.

65   Above all, we will prepare the PLRs according to our previous report and use PA as a flame retardant,

66 in order to obtain the PCM with enhanced tensile properties and FR performance, and promote its

67 practical application accordingly. The tensile properties, fire-safety, shape memory properties and phase

68 transition performance of the composites will be investigated and explore the potential applications of

69 the PCMs in thermal management of electronic devices.

70 2. EXPERIMENTAL

71 *Materials.* Poly (ethylene oxide) (PEO) with a weight average molar mass of 9×10^5 g mol^{-1}, α-

72 Cyclodextrin (α-CD, ≥99.8%) and phytic acid (PA, 50 wt.%) were purchased from Sigma Aldrich (USA)

73 and used without further treatment. Deionized water is made in our laboratory.

74 *Synthesis of polyrotaxane (PLR).* PEO (3 g) was dissolved in H$_2$O (80 mL) at 80 °C, and then α-CD (0.9

75 g) with different mass ratio 30% was slowly added. After stirring for overnight at room temperature,

76 the reaction mixture was cooled down and kept at 4 °C for 72 h to yield the corresponding inclusion

77 complex solutions.

78 *Preparation of PA modified PLR (PLR-PA) films*. The aqueous **PLR-PA** (with different contents of PA)

79 and pure PLR solution were casted directly into 10×10 cm^2 Polytetrafluoroethylene (PTFE) mold. After

80 evaporation at room temperature, the flexible films (PLR (sample without PA), PLR-PA10

81 (PLR/PA=100/10 (w/w)), PLR-P20 (PLR/PA=100/20 (w/w)) and PLR-PA30 (PLR/PA=100/30 (w/w)))

82 were further dried under 100 °C for 6 h to remove the water. Finally, the films with thickness at about

83 0.1 mm were obtained by hot press (R-320 22015, QIEN, Wuhan, China, 150 °C, 10-20 MPa, 5 min).

84 *XRD* patterns of the films were recorded in reflection mode using a X'PERT-PRO diffractometer with

85 Cu Kα (λ=0.1542 nm) and Ni filter.

86 *ATR–FTIR* spectra of the films were recorded from 500 cm^{-1} to 4000 cm^{-1} using Jasco FT/IR-6100 at

87 room temperature.

88 *DSC* test was performed by using a TA-Q200 in a N$_2$ atmosphere (50 mL min^{-1}). The crystallinity (φ_c%)

89 were calculated in the second heating run from -60 °C to 100 °C at heating rate of 10 °C min^{-1} by the

90 equation:

91
$$\varphi_c\% = \frac{\Delta H_m}{\omega_i \Delta H_m^0} \times 100\% \tag{1}$$

92   where, ΔH_m (J g^{-1}) represented the measured enthalpies of melting, ΔH_m^0 (J g^{-1}) was the melting

93   enthalpy for a complete crystalline polymer and ω_i was the weight content of the component i in the

94   sample. The ΔH_m^0 of PEO was 196.4 J g^{-1}.

95   *Cycle stability test*. Sample PLR-PA10 was selected for cycle stability test (100 cycles). Both heating

96   and cooling procedures were run from -10 ºC to 90 ºC at 10 °C min^{-1} to calculate the change of

97   exothermic and endothermic heat as well as the enthalpy efficiency and phase change temperatures.

98   *UV-Vis Absorption Spectrometry*. A UV-2600 (SHIMADZU Corp., Kyoto, Japan) spectrophotometer

99   was used for the determination of UV-vis transmittance spectra for the film with thickness at 0.1 mm.

100   *TGA* of the films was performed using a TGA in air atmosphere from 25 °C to 600 °C at 10 °C min^{-1}

101   using a TA-Q50 instrument.

102   *Form stability*. The sample was cut into a disc of 13.50 ± 0.05 mm with a cutter, and then heated at

103   different temperatures (30 ºC and 80 ºC) for the detecting of form stability (leakage or shape change).

104   SEM and EDS were carried out on the apparatus (SEM, EVO MA15, Zeiss) and FIB-FEG SEM dual-

105   beam microscope (Helios NanoLab 600i, FEI).

106   *Tensile test*. The tensile test samples were dogbone-shaped, following with ISO 527-2 (1996) standard.

107   An Instron 5966 (USA) universal tensile testing machine was utilized at a rate of 50 mm·min^{-1}.

108   Minimum 5 specimens were tested for each sample to obtain a reliable average value and standard

109   deviations.

110   *Fire resistance*. Samples with diameter of 13.5 mm were sent to the top of a flame, and a camera was

111   used to record combustion process.

112   *The fire behavior*. The fire behavior was investigated by cone calorimeter test according to ISO5660

113   (heat flux is 35 kW·m^{-2}). Limiting oxygen index (LOI) test was performed based on standard ASTM D

114   2863-77. The vertical burning test was carried on UL-94 vertical flame chamber according to ASTM

115   D3801.

116   *Thermal conductivity*. Thermal conductivity measurements were performed using a thermal constants

117   analyzer (TPS2500 S, Hot Disk) at room temperature. The sample is with thickness of ~4 mm.

118   *Shape Memory performance*. Each sample was cut from a film with dimensions 30 mm ×2.5 mm ×0.1

119   mm. The percentage of shape fixing ratio (R_f), and shape recovery (R_r), were calculated according to

120   the following equations:

121    $$R_f(N) = \frac{l_f(N)-l_i(N-1)}{l_p(N)-l_i(N-1)} \times 100\% \qquad (2)$$

122    $$R_r(N) = \frac{l_p(N)-l_r(N)}{l_p(N)-l_i(N-1)} \times 100\% \qquad (3)$$

123   where l_p was the length before releasing the applied load, l_f was the length obtained after releasing the

124   applied load, l_i was the initial sample length, and l_r was the final length after heating with no applied

125   load. N is the cycle number. Three cycles were included in the test, namely, C1, C2 and C3.

126   3. RESULTS AND DISCUSSION

127   *3.1 Preparation and characterization of PLR-PA*
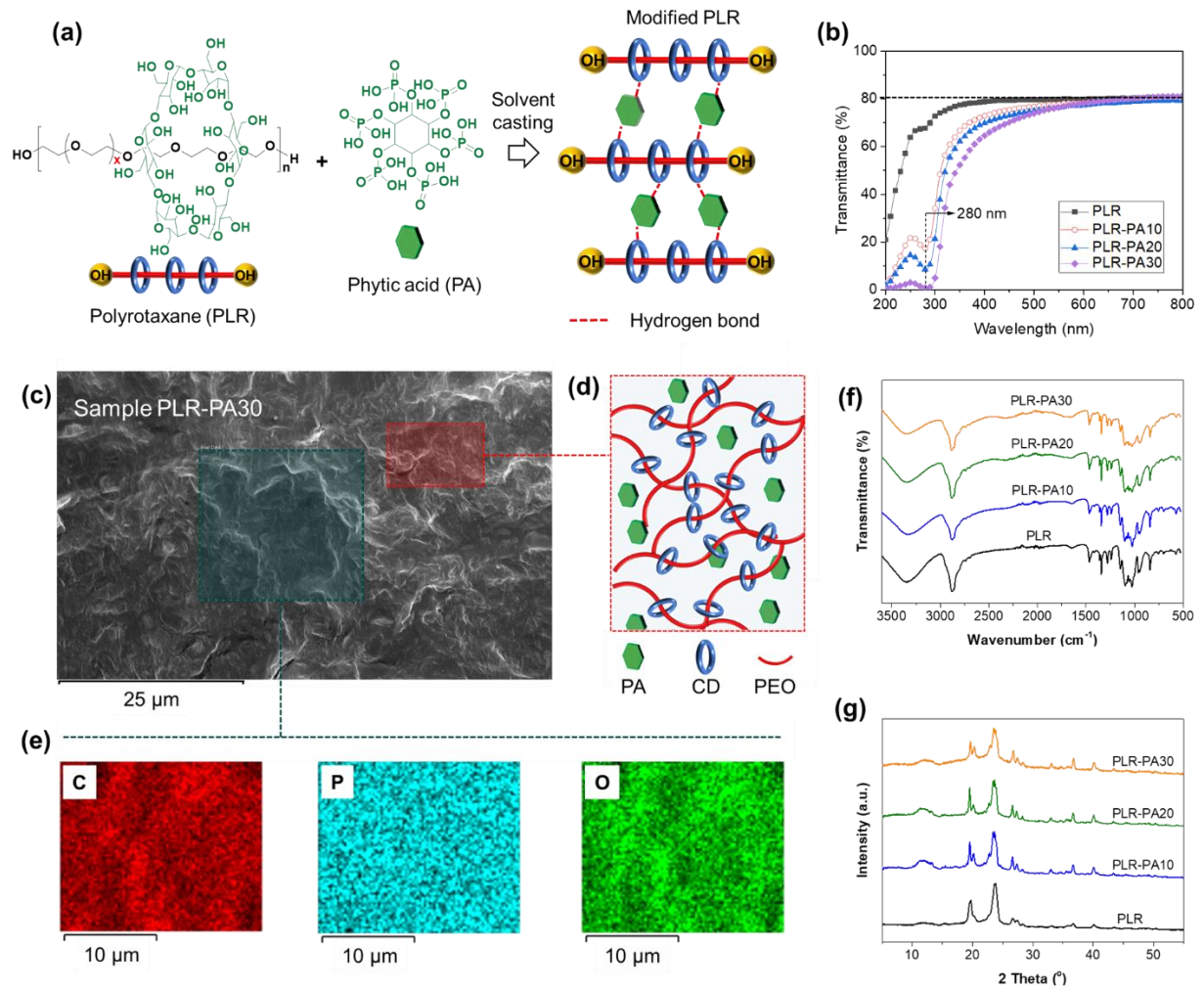
Fig. 1. (a) PLR-PAs fabrication route by solvent blending casting, (b) UV-Vis spectra of PLR and PLR-PAs, (c) SEM cross section image of PLR-PA30; (d) illustration of PA dispersion; (e) EDX mapping of C, P and O element, (f) FTIR spectra of PLR and PLR-PAs and (g) XRD curves of the four samples.

PLR-30% with high form stability and melting enthalpy was synthesized according to our previous work [29] and selected as reference in current work for evaluation of PA effect on the systematic performance on the PLR-30%. The biomass PA (**Fig. 1a**) is blended directly with the PLR by using solvent casting method, for obtaining the PA functionalized PLR (PLR-PA) (**Fig. 1a**). **Fig. 1b** shows the UV–vis spectra of the PLR and PLR-PA sheets with thickness of 0.1 mm. All the PCM sheets

138   showed a high transmittance of ~80% at the wavelength of 500-800 nm, which indicates the addition

139   of PA didn't change the PLR transparency remarkably.

140   Both PA and PLR (with a lot of α-CD rings) are polyhydroxy compounds. The hydrogen bond

141   interaction between PLR (both PEO and α-CD) and PA can make sure the good dispersion of PA in

142   the PLR matrix. PLR-PA30 was selected as a typical example for the PA dispersion analysis (**Fig. 1c**).

143   There is no significant PA aggregation, as further illustrated in **Fig. 1d**. The PA has good compatibility

144   with PLR and is easy to be dispersed in the PLR matrix, which can be directly proved by the EDX

145   results (**Fig. 1e**). The FTIR spectra are shown in **Fig. 1f**. There is no obvious difference among all the

146   FTIR curves.

147   In **Fig. 1g**, the two significant peaks at 2θ angles of about 19° and about 23° are attributed to the (120)

148   and (032) planes, respectively. The crystallinity ($\varphi_c\%$) were calculated by the **Eq. 4**:[36]

149    $$\varphi_c\% = \frac{\Delta H_m}{\omega_i \Delta H_m^0} \times 100\% \tag{4}$$

150   where, ΔH_m (J g^{-1}) represented the measured enthalpies of melting, ΔH_m^0 (J g^{-1}) was the melting

151   enthalpy for a 100 % crystalline PEO and ω_i was the fraction of the component *i* in the sample. The

152   ΔH_m^0 of PEO was 196.4 J g^{-1}. [37] The results were listed in **Table S1**. We found that with the increase

153   of PA content, the crystallinity of the material decreased slightly. However, it can be maintained at

154   about 50%, which is also a prerequisite to ensure that the material has phase change thermal regulation.

155   *3.2 Mechanical performance*
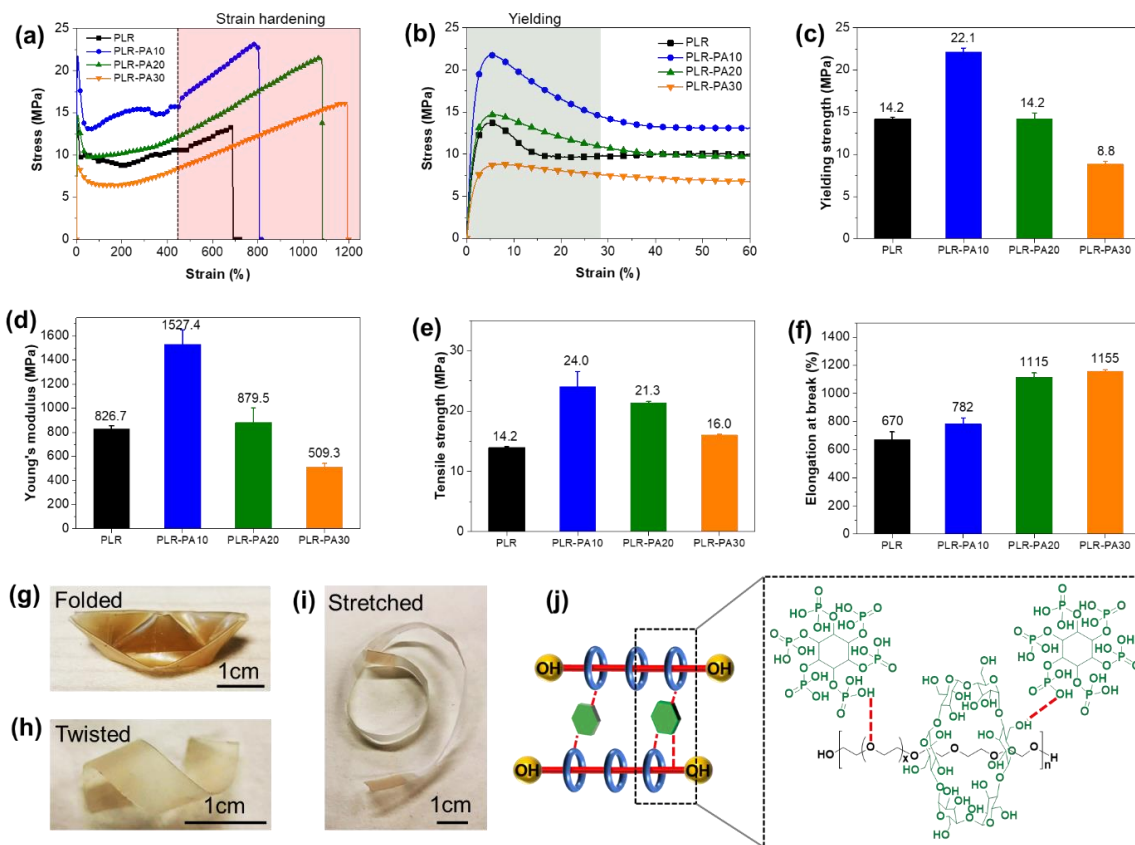
Fig. 2. (a) full range stress-strain curves, (b) stress-strain curves at low strain region, (c) yielding strength, (d) Young's moduli, (e) tensile strength, (f) elongation at break of the PCM samples, (g) boat-shape folded sample, (h) twisted sample, (i) stretched sample and (j) hydrogen bond (the red dotted line) illustration between PA and both PEO chain and α-CD ring.

Tensile test curves of the four PCM sheets are shown in **Fig. 2a**. The detailed values for the parameters are summarized in **Table S2**. The samples show obvious yielding **(Fig. 2b)** and remarkable strain hardening (Fig. 2a). It is found that the yielding strength (**Fig. 2c**), Young's modulus (**Fig. 2d**), and tensile strength (**Fig. 2e**) of the materials increased at first and then decreased with the increase of PA contents. The elongation increased steadily with the increase of PA contents. PLR-PA10 can reach the top values for all the Young's Modulus (1527.4 MPa), tensile strength (24.0 MPa) and Yielding strength

169   (22.1 MPa). It is probably due to the excellent PA dispersion and the intramolecular hydrogen bond. It

170   is clearly depicted in **Fig. 2g-i** that the samples can be easily deformable (twisting, folding, and

171   stretching). As shown in **Fig. 2j**, the interactions between PA and α-CD may be hydrogen bond between

172   α-CD in both PLR and PLRs. In addition, the oil-like additive can maintain the formability, which will

173   benefit in the mechanical properties maintaining during tension.[32]

174   *3.3 PCMs performance and shape memory properties*

175   **Table 1**. Some core parameters of PCMs

Samples	ΔH_m (J g^{-1})	Enthalpy efficiency (%)	ΔE_a (kJ mol^{-1})	Extent of Supercooling (°C)	Heat lose (%)	Thermal conductivity (W m^{-1} k^{-1})	Form stability
PLR	88.6	99.9	571.1	10.0	2.1	0.28±0.03	No leakage
PLR-PA10	79.2	97.4	229.5	11.6	3.7	0.32±0.02	No leakage
PLR-PA20	68.3	89.5	475.9	15.3	1.4	0.34±0.04	No leakage
PLR-PA30	60.9	84.5	342.4	16.1	3.6	0.37±0.03	No leakage

176
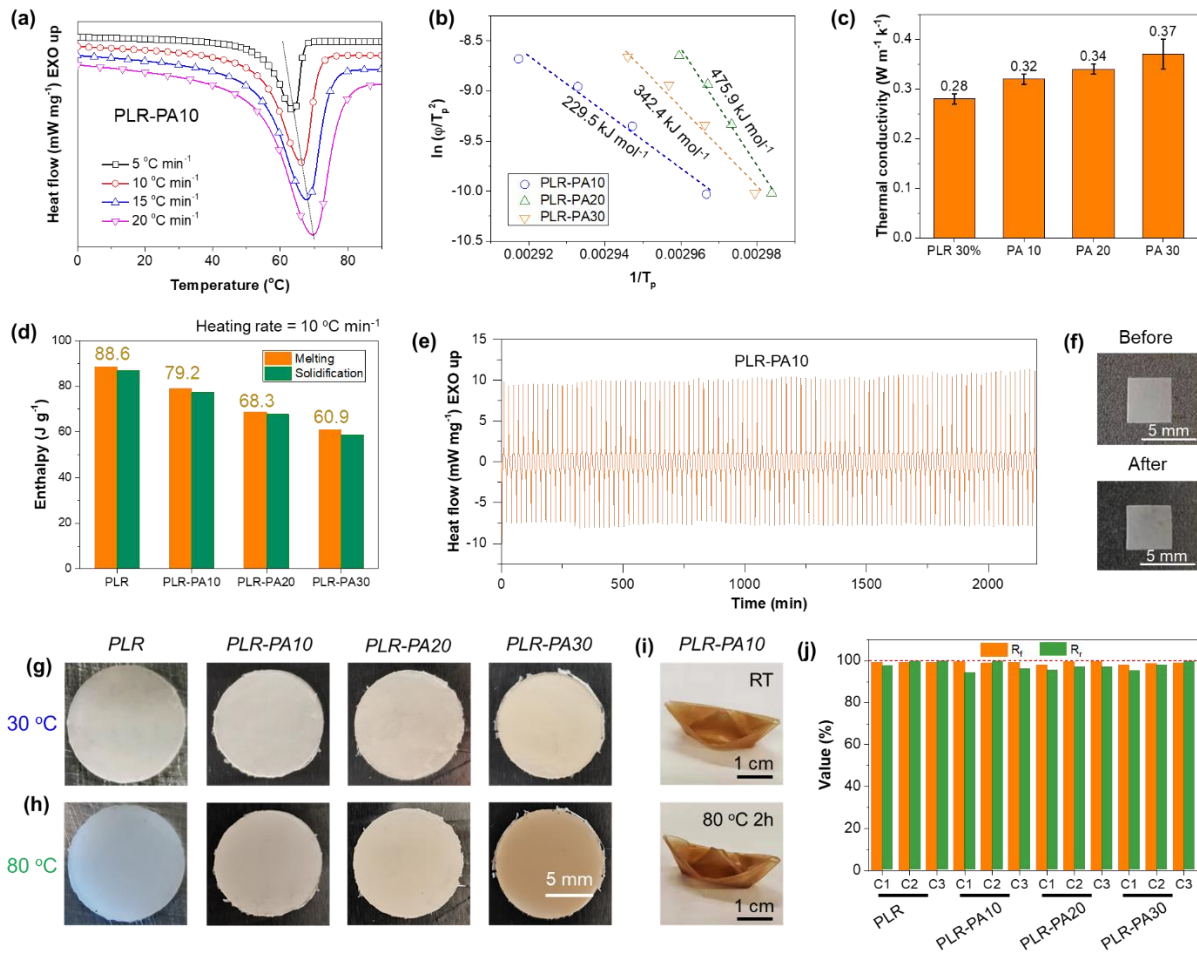
Fig. 3. (a) DSC curves for second heating of PLR-PA10 with four different heating rates, (b) $\ln(\emptyset/T_p^2)$-$1/T_p$ plots;

(c) thermal conductivity results; (d) melting results of the PCMs; (e) DSC curves of PLR-PA10 after 100 times

thermal/cooling cycling; (f) the images of PLR-PA10 before and after thermal cycling test by DSC equipment;

form stability and leakage proof test of the PCMs: (g) 30 °C, and (h) 80 °C for 2 h, (i) Image of boat shape sample

PLR-PA10 before and after heat treatment, and (j) R_f and R_r values of the PCMs.

Kissinger equation was used to calculate the activation energy (ΔE_a, kJ mol^{-1}). Considering an

homogenous transformation at the phase change, the Kissinger equation reads [38],

$$\frac{d[ln(\varphi/T_P^2)]}{d(\frac{1}{T_P})} = -\frac{\Delta E_a(T)}{R} + T_p \ln(-\frac{AR}{E} f'(\alpha)) \tag{5}$$

187 where φ is the heating rate, T_P is the phase transition temperature. The detected T_P with different

188 heating rate are all listed in **Table S3**). A is the pre-exponential term in the Arrhenius kinetic, $f(\alpha)$ is

189 the transformation function at phase change and R is the gas constant. Typically, the Kissinger method

190 determines the activation energy considering the left-hand term and the first right-hand term in Eq. (5),

191 being then, the second right-hand term negligible. On a practical sound, this is acceptable provided the

192 quotient $\frac{\Delta E_a}{RT_p} > 10$, leading to an estimated modelling error below 2%. [39] In addition, this reflects

193 that the associated kinetic function rate of change in the proximity of the transformation is well

194 approximately constant. **Fig. 3a** shows the melting curves of PLR-PA10. The curves of samples PLR-

195 PA20 and PLR-PA30 are provided in Fig. S1-2. **Fig. 3b** presents the Kissinger plots. It is reported that

196 $\Delta E_{a,PLR}$=571.1 kJ mol^{-1} for PLR. [29] In current work, the following Δ E$_a$ were obtained: $\Delta E_{a, PLR-}$

197 $_{PA10}$=229.5 kJ mol^{-1}, $\Delta E_{a, PLR-PA20}$=475.9 kJ mol^{-1}, and $\Delta E_{a, PLR-PA30}$=342.4.0 kJ mol^{-1} for PLR-PA10%,

198 PLR-PA20% and PLR-PA30%, respectively. We found that all the ΔE_a of the PLRs are much lower

199 than that of neat PLR, which is probably because the PA will promote the mobility process of PEO in

200 the PCMs. For each ΔE_a obtained, the quotient $\frac{\Delta E_a}{RT_p} > 10$ which permits the use of the Kissinger

201 equation (2) disregarding the kinetic term.

202 The extent of supercooling (ΔT, ^oC) can be calculated by **Eq. 3**:

203
$$\Delta T = T_{m,onset} - T_{s,onset} \tag{6}$$

204 The calculated ΔT is summarized in **Table 1**. The ΔT increased slightly with the increase of PA

205 contents, indicating that the high PA contents will hinder the nucleation process of PEO chain. **Eq. 7**

206 was used to determine the Enthalpy efficiency of PCMs: [10, 40]

207
$$Enthalpy\ efficiency\ \% = \frac{\Delta H_m}{\omega \Delta H_{PCM}} \times 100\ \% \tag{7}$$

208   where, ΔH_m was the melting enthalpy of the PCMs. ΔH_{PCM} was the enthalpy of pure PLR, and ω

209   was the mass ratio of PLR in the PCMs.

210   The heat lose (η, %) can be calculated by **Eq. 8**:

211    $$\eta = \frac{\Delta H_m - \Delta H_s}{\Delta H_m} \times 100\ \%$$ (8)

212   where, ΔH_m (J g^{-1}) was the melting enthalpy, and ΔH_s (J g^{-1}) is solidification enthalpy. **Table 1** and

213   **Table S1** summarizes the thermal parameters of PLR and PLR-PAs, such as ΔH_m, $T_{m,onset}$, ΔH_s, and

214    $T_{S,\ onset}$. It is found that the thermal conductivity of the PCM increased slightly with the increase of PA

215   contents, the values of which were listed in Table 1 and shown in **Fig. 3c**. The PCMs exhibited a melting

216   enthalpy (60.9~79.2 J g^{-1}, **Fig. 3d**) and high enthalpy efficiency. The corresponding DSC curves during

217   heating and cooling were provided in Figure S3-S6. Notably, according to **Eq. 8**, the heat loss for all

218   the samples is also listed in **Table 1**. All the η for PLR were quite low (<3.7%), which indicated PA

219   will not significantly induce the heat dissipation for the PCMs. The PCMs films had high cycle

220   performance because the ΔH_m and ΔH_s, et al., were almost unchanged (**Fig. 3e** and **Table 1**). DSC

221   test sample has excellent shape retention after 100 cycles (**Fig. 3f**), indicating it is suitable for long-

222   term application stably.

223   The photos of PLR and PLR-PAs before and heat treatment are shown in **Fig. 3 g** and **Fig. 3 h**. No

224   leakage neither shape change (Fig. 4i) was observed during the heating process even when the

225   temperature was much higher than the corresponding T_m, which indicates that the PLRs have excellent

226   form stability and leakage-proof performance. Furthermore, it is found the PCMs show outstanding

227   SMPs. The detail shape memory results are all listed in **Table S4**. Notably, the R_f is higher than 98 %

228   of the initial strain after unloading of the stress, and the recovery ratio (R_r) is higher than 95 % as shown

229   in **Figure 3j**.

230

3.4 Thermal stability, fire safety and application

232
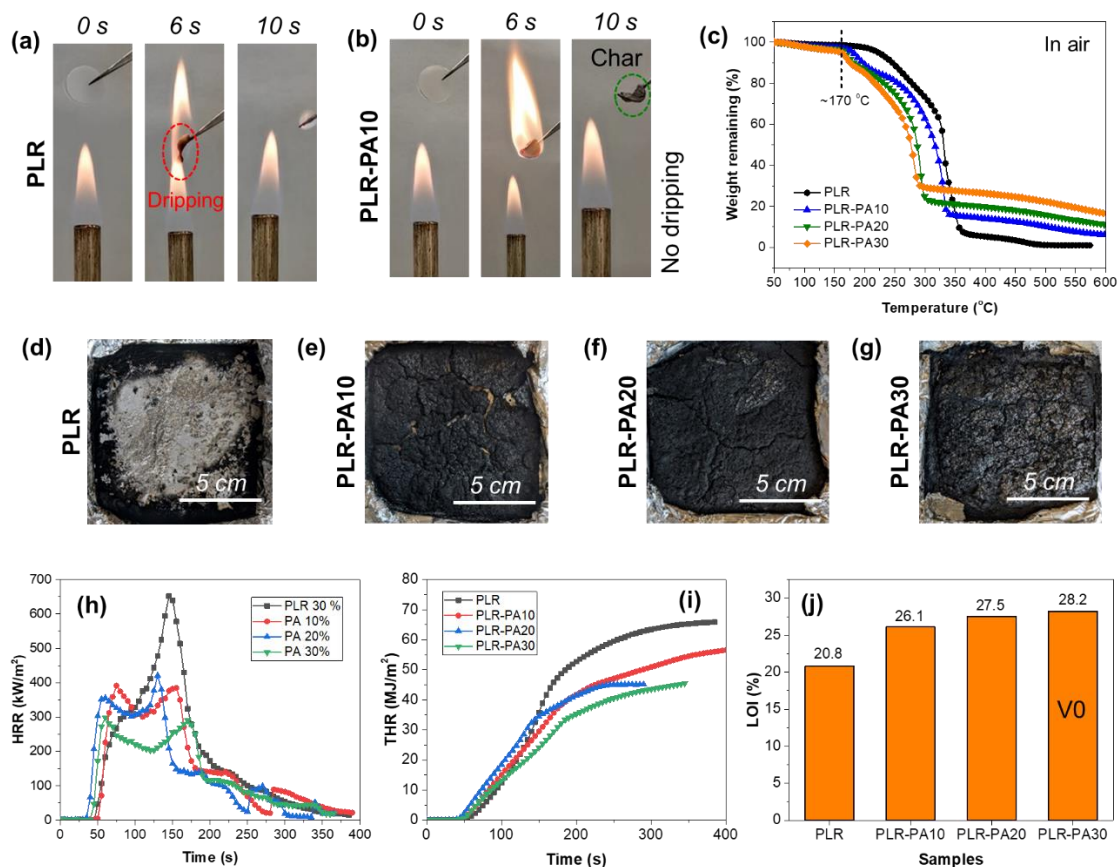
Fig. 4. Combustion images of sample (a) PLR, (b) sample PLR-PA10, (c) TGA curves of all the PCM

samples, (d) char morphology of sample PLR, (e) char morphology of sample PLR-PA10, (f) char

morphology of sample PLR-PA20, (g) char morphology of sample PLR-PA30, (h) HRR curves of all

the PCMs, (i) THR curves of all the PCMs, and (j) LOI values of the PCMs.

237

The combustion process of the four samples were shown in **Fig. 4a-4b** and **Fig. S3**. As a control sample,

pristine PLR produced obvious dripping (at 6s, **Fig. 4a**). All the PA functionalized PCMs have a stable

char residue (**Fig. 4 b and Fig. S7**) and show no dripping. During combustion, no dripping may slow

down the fire spread to a certain extent, and accordingly improve the flame retardancy.

15

242   Subsequently, TGA results are recorded and presented in **Fig. 4c** and **Table S5**. As it can be seen, all

243   the modified PCMs typically underwent a two-step decomposition process. The weight loss near 200

244   ºC is mainly due to PA decomposition. [41] It is clearly seen that all the functionalized PLRs

245   decomposes earlier in comparison with PA, which begins to decompose after 170 ºC. The weight loss

246   in the first stage (170 ~ 220 ºC) is due to the PA decomposition, which is in consistent with the report

247   that the earlier start of decomposition with a higher char residue is often found for samples with good

248   flame retardancy. [42] [43, 44]

249   CONE was further used to characterize the fire safety of the materials. **Fig. 4d** to **4g** present the char

250   morphology of sample PLR, PLR-PA10, RLR-PA20 and PLR-PA30. This is consistent with the change

251   trend of residue in TGA, that is, the residual carbon content increases with the increase of PA content.

252   Most importantly, the pHRR of PLRs decreased with the increase of PA content. For PLR-PA30, the

253   pHRR was decreased by 54.2 %, and THR decreased by 34.0 % than that of PLR. The change trend of

254   THR can be seen intuitively in **Fig. 4g**. The specific data are listed in **Table 2**. It is clear from the results

255   that the fire safety of the modified material is improved due to the decrease of both pHRR and THR

256   significantly. LOI and UL-94 tests were recorded and the results are shown in **Fig. 4j** and **Table 2**. With

257   the addition of 30 wt.% PA, the LOI values increased from 20.8% to 28.2% and the PCM reached a V-

258   0 rating for the UL-94 test. We can understand the flame retardancy mechanism based on the well

259   reported statement elsewhere. Typically, during the combustion, PA often acted as the acid source in the

260   flame retardant system. In addition, the PA generates many non-combustible gases, produces

261   phosphorus-containing free radicals, and captures the free radical ions in the system in the gas phase.

262   At the same time, a large amount of phosphorus in its structure can be used as a charring agent to

263   promote the formation of more stable carbon residue in the system.[45] Cyclodextrin in PLR will be

264 dehydrated and carbonized during combustion to produce a large amount of carbon residue.[46] As a

265 physical barrier, the carbon layer effectively insulates the transmission of oxygen and heat and plays an

266 essential role in the flame retardance of the condensed phase.

267 **Table 2.** The char residue, TGA and typical parameters for CONE test, UL-94 and LOI

Samples	Residue (%) by TGA	pHRR (kW m^{-2})	THR (MJ m^{-2})	LOI (%)	UL-94	Dripping
PLR	1.1	652	65.9	20.8	No rating	Yes
PLR-PA10	6.5	391	52.5	26.1	No rating	No
PLR-PA20	11.4	420	46.0	27.5	No rating	No
PLR-PA30	16.5	298	44.0	28.2	V0	No

268

269 **Table 3**. Thermal properties of as-prepared composite PCMs and recently bio-based fire safe PCM
270 composites

Year	PCM compositions	Flexible	Bio-based	Flame Retardants	Latent heat (J g^{-1})	LOI increase (%)	pHRR decrease (%)	References
2019	Bio-char/Paraffin	No	Yes	-	25.2-92.1	-	-	[47]
2019	Bio-waste/Nature soy-wax or Golden soy-wax	No	Yes	-	19.4-21.1	-	-	[48]

2020	Oilseed straw or Miscanthus straw/n-dodecane or 1-dodecanol	No	Yes	--	54.1-90.5	-	-	[49]
2010	HDPE/Paraffin	Yes	No	Expanded graphite	68.3-81.5	N/A	-62.0%	[14]
2010	HDPE/Paraffin	Yes	No	Chlorinated paraffin	49.6-70.1	N/A	-61.2%	[50]
2021	PGI/PEG	No	Yes	APP	70.1-86.9	+21.4%	-36.1%	[5]
2022	PLR	Yes	Yes	PA	60.9-79.2	+35.6%	-54.2%	This work

271

Some PCM key parameters in some other reports are listed in **Table 3**. Through comparison, we found

that the significant progress of this work is reflected in: (1) efficient and green fabrication by using

water as the only solvent, (2) Biobased, flexible and smart nature of the PCMs (3) excellent flame-

retardant performance. Therefore, the material is expected to be applied safely in the sustainable field

of temperature control of flexible electronic devices.

277
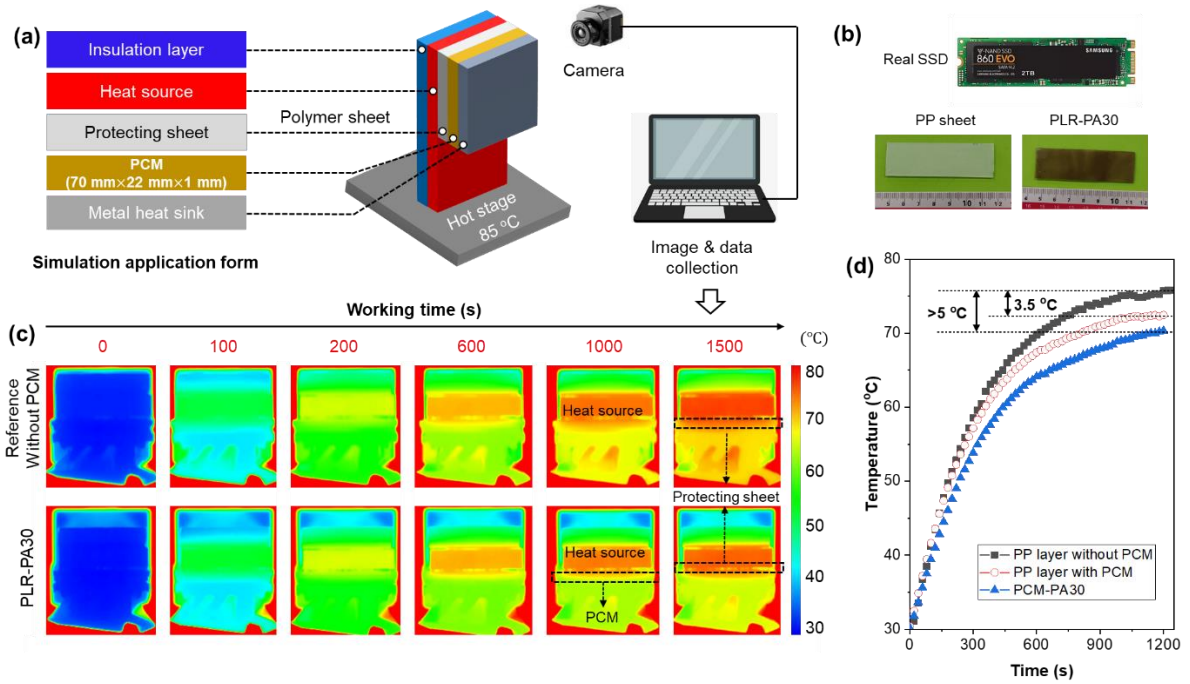
Fig. 5. (a) The device stack structure and test process, (b) the image of real Solid-State Disk (SSD), Polypropylene (PP, with thickness of 2 mm) sheet and PLR-PA30, (c) IR images of the simulated devices, (d) the temperature increasing curves of the devices.

To evaluate the heat management of the PCM on the electronic devices, we designed a schematic structure (Fig. 5a). The insulation layer (with thickness of 5 mm), heating source, protecting sheet (PP), PCM (Fig. 5b), and the metal heatsink stacked together to prepare the simulated device. Fig. 5c shows the IR images of samples A and B. Based on the IR images, we can further measure the temperature tendency (Fig. 5d). Notably, the curve of each sample here is drawn based on the average values with 3 parallel tests, which can ensure the repeatability of the data. As shown in Fig. 5d, during the heating, sample PLR-PA30 showed significantly better heat control state than that of both the blank samples and commodities. Typically, the temperature of the protecting part with PCM was obviously lower than that of blank sample. Furthermore, during the phase transition, the temperature difference gradually

292 appears and keep relatively constant at about 3.5 °C. We assigned that the difference is because of the

293 latent heat of PLR-PA30, which plays a key role in heat management.

294

295 4. CONCLUSIONS

296 PLR with different PA contents (10%-30%) were prepared by using a green physical blending method.

297 Compared with the pristine PLR, all the Young's modulus, tensile strength and yielding strength of the

298 PLR-PAs increased at first and then decreased with the increase of PA contents. Typically, the Young's

299 modulus, yielding strength and tensile strength of the PLR were 826.7 MPa, 14.2 MPa and 14.2 MPa,

300 respectively, and significantly increased to 1527.4 MPa, 22.1 MPa, and 24.0 MPa respectively, with the

301 addition of 10 wt.% of PA. Elongation (>783 %) for all modified PCMs was gradually increased with

302 the increase of PA contents. Thermal analysis shows that the fire safety of PLR is significantly improved.

303 Specifically, for the best sample PLR/PA30, the pHRR could decrease by 54.2 %, THR decreased by

304 34.0%; the char residual increased from 1.1% to 13.6 % and the LOI increased from 20.8% to 28.2%;

305 moreover, the stable char residual will be formed during combustion process. The PCMs showed high

306 shape-fixing ratio (R_f >98%) and recovery ratio (R_r >95 %). Further with the excellent form-stability

307 and good cycle performances, the modified PLRs are therefore fire safe, ultra-flexible, sustainable, and

308 advanced PCMs for energy storage.

309

310 **Supporting Information**.

313 **References**

20

[1] G. Ye, G. Zhang, L. Jiang, X. Yang, Temperature control of battery modules through composite phase change materials with dual operating temperature regions, Chemical Engineering Journal 449 (2022) 137733.

[2] Y. Lv, X. Yang, G. Zhang, Durability of phase-change-material module and its relieving effect on battery deterioration during long-term cycles, Applied Thermal Engineering 179 (2020) 115747.

[3] K. Iqbal, A. Khan, D. Sun, M. Ashraf, A. Rehman, F. Safdar, A. Basit, H.S. Maqsood, Phase change materials, their synthesis and application in textiles—a review, The Journal of The Textile Institute 110(4) (2019) 625-638.

[4] T.R. Whiffen, S.B. Riffat, A review of PCM technology for thermal energy storage in the built environment: Part I, International Journal of Low-Carbon Technologies 8(3) (2012) 147-158.

[5] G.-Z. Yin, X.-M. Yang, J. Hobson, A.M. López, D.-Y. Wang, Bio-based poly (glycerol-itaconic acid)/PEG/APP as form stable and flame-retardant phase change materials, Composites Communications 30 (2022) 101057.

[6] B. Wang, G. Li, L. Xu, J. Liao, X. Zhang, Nanoporous Boron Nitride Aerogel Film and Its Smart Composite with Phase Change Materials, ACS Nano 14(12) (2020) 16590-16599.

[7] W. Wu, G. Ye, G. Zhang, X. Yang, Composite phase change material with room-temperature-flexibility for battery thermal management, Chemical Engineering Journal 428 (2022) 131116.

[8] Z. Cai, J. Liu, Y. Zhou, L. Dai, H. Wang, C. Liao, X. Zou, Y. Chen, Y. Xu, Flexible phase change materials with enhanced tensile strength, thermal conductivity and photo-thermal performance, Solar Energy Materials and Solar Cells 219 (2021) 110728.

[9] Q. Huang, X. Li, G. Zhang, J. Deng, C. Wang, Thermal management of Lithium-ion battery pack through the application of flexible form-stable composite phase change materials, Applied Thermal Engineering 183 (2021) 116151.

[10] P. Cheng, H. Gao, X. Chen, Y. Chen, M. Han, L. Xing, P. Liu, G. Wang, Flexible monolithic phase change material based on carbon nanotubes/chitosan/poly(vinyl alcohol), Chemical Engineering Journal 397 (2020) 125330.

[11] Y. Kou, K. Sun, J. Luo, F. Zhou, H. Huang, Z.-S. Wu, Q. Shi, An intrinsically flexible phase change film for wearable thermal managements, Energy Storage Materials 34 (2021) 508-514.

[12] L. Li, G. Wang, C. Guo, Influence of intumescent flame retardant on thermal and flame retardancy of eutectic mixed paraffin/polypropylene form-stable phase change materials, Applied Energy 162 (2016) 428-434.

[13] G. Song, S. Ma, G. Tang, Z. Yin, X. Wang, Preparation and characterization of flame retardant form-stable phase change materials composed by EPDM, paraffin and nano magnesium hydroxide, Energy 35(5) (2010) 2179-2183.

[14] P. Zhang, Y. Hu, L. Song, J. Ni, W. Xing, J. Wang, Effect of expanded graphite on properties of high-density polyethylene/paraffin composite with intumescent flame retardant as a shape-stabilized phase change material, Solar Energy Materials and Solar Cells 94(2) (2010) 360-365.

[15] M.J. Mochane, A.S. Luyt, Synergistic effect of expanded graphite, diammonium phosphate and Cloisite 15A on flame retardant properties of EVA and EVA/wax phase-change blends, Journal of Materials Science 50(9) (2015) 3485-3494.

[16] M.J. Mochane, A.S. Luyt, The effect of expanded graphite on the thermal stability, latent heat, and flammability properties of EVA/wax phase change blends, Polymer Engineering & Science 55(6) (2015) 1255-1262.

[17] J. Wang, Y. Wang, R. Yang, Flame retardance property of shape-stabilized phase change materials, Solar Energy Materials and Solar Cells 140 (2015) 439-445.

[18] S.A. Isarov, P.W. Lee, J.H. Towslee, K.M. Hoffman, R.D. Davis, J.M. Maia, J.K. Pokorski, DNA as a flame

358 retardant additive for low-density polyethylene, Polymer 97 (2016) 504-514.

359 [19] J. Alongi, A.D. Blasio, F. Cuttica, F. Carosio, G. Malucelli, Bulk or surface treatments of ethylene vinyl

360 acetate copolymers with DNA: Investigation on the flame retardant properties, European Polymer Journal 51

361 (2014) 112-119.

362 [20] R. Chen, Z. Luo, X. Yu, H. Tang, Y. Zhou, H. Zhou, Synthesis of chitosan-based flame retardant and its fire

363 resistance in epoxy resin, Carbohydrate Polymers 245 (2020) 116530.

364 [21] Y. Wang, C. Liu, J. Lai, C. Lu, X. Wu, Y. Cai, L. Gu, L. Yang, G. Zhang, G. Shi, Soy protein and halloysite

365 nanotubes-assisted preparation of environmentally friendly intumescent flame retardant for poly(butylene

366 succinate), Polymer Testing 81 (2020) 106174.

367 [22] M.N. Prabhakar, A.u. Rehman Shah, J.-I. Song, Improved flame-retardant and tensile properties of

368 thermoplastic starch/flax fabric green composites, Carbohydrate Polymers 168 (2017) 201-211.

369 [23] Z. Liu, S. Shang, K.-l. Chiu, S. Jiang, F. Dai, Fabrication of conductive and flame-retardant bifunctional

370 cotton fabric by polymerizing pyrrole and doping phytic acid, Polymer Degradation and Stability 167 (2019)

371 277-282.

372 [24] X. Liu, Q. Zhang, B. Peng, Y. Ren, B. Cheng, C. Ding, X. Su, J. He, S. Lin, Flame retardant cellulosic

373 fabrics via layer-by-layer self-assembly double coating with egg white protein and phytic acid, Journal of

374 Cleaner Production 243 (2020) 118641.

375 [25] X.-W. Cheng, J.-P. Guan, X.-H. Yang, R.-C. Tang, F. Yao, A bio-resourced phytic acid/chitosan

376 polyelectrolyte complex for the flame retardant treatment of wool fabric, Journal of Cleaner Production 223

377 (2019) 342-349.

378 [26] W. Guo, X. Wang, J. Huang, Y. Zhou, W. Cai, J. Wang, L. Song, Y. Hu, Construction of durable flame-

379 retardant and robust superhydrophobic coatings on cotton fabrics for water-oil separation application, Chemical

380 Engineering Journal 398 (2020) 125661.

381 [27] C.V.S. Rosely, A.M. Joseph, A. Leuteritz, E.B. Gowd, Phytic Acid Modified Boron Nitride Nanosheets as

382 Sustainable Multifunctional Nanofillers for Enhanced Properties of Poly(l-lactide), ACS Sustainable Chemistry

383 & Engineering 8(4) (2020) 1868-1878.

384 [28] D. Wang, Y. Wang, T. Li, S. Zhang, P. Ma, D. Shi, M. Chen, W. Dong, A Bio-Based Flame-Retardant Starch

385 Based On Phytic Acid, ACS Sustainable Chemistry & Engineering 8(27) (2020) 10265-10274.

386 [29] G.-Z. Yin, J. Hobson, Y. Duan, D.-Y. Wang, Polyrotaxane: New generation of sustainable, ultra-flexible,

387 form-stable and smart phase change materials, Energy Storage Materials 40 (2021) 347-357.

388 [30] G.-Z. Yin, A. Marta López, X.-M. Yang, X. Ao, J. Hobson, D.-Y. Wang, Polyrotaxane based leakage-proof

389 and injectable phase change materials with high melting enthalpy and adjustable transition temperature,

390 Chemical Engineering Journal 444 (2022) 136421.

391 [31] G.-Z. Yin, A. Marta López, X.-M. Yang, W. Ye, B. Xu, J. Hobson, D.-Y. Wang, Shape-stable and smart

392 polyrotaxane-based phase change materials with enhanced flexibility and fire-safety, European Polymer Journal

393 173 (2022) 111262.

394 [32] G.-Z. Yin, X. Yang, Z. Zhou, Q. Li, A Green Pathway to Adjust the Mechanical Properties and Degradation

395 Rate of PCL by Blending Bio-sourced Poly (Glycerol-Succinate) Oligoesters, Materials Chemistry Frontiers

396 (2017).

397 [33] Y. Yang, X. Zhao, J. Yu, X. Chen, X. Chen, C. Cui, J. Zhang, Q. Zhang, Y. Zhang, S. Wang, Y. Cheng, H-

398 Bonding Supramolecular Hydrogels with Promising Mechanical Strength and Shape Memory Properties for

399 Postoperative Antiadhesion Application, ACS Applied Materials & Interfaces 12(30) (2020) 34161-34169.

400 [34] Y.-N. Chen, L. Peng, T. Liu, Y. Wang, S. Shi, H. Wang, Poly(vinyl alcohol)–Tannic Acid Hydrogels with

401 Excellent Mechanical Properties and Shape Memory Behaviors, ACS Applied Materials & Interfaces 8(40)

402   (2016) 27199-27206.

403   [35] S. Yang, Y. Zhang, T. Wang, W. Sun, Z. Tong, Ultrafast and Programmable Shape Memory Hydrogel of

404   Gelatin Soaked in Tannic Acid Solution, ACS Applied Materials & Interfaces 12(41) (2020) 46701-46709.

405   [36] G. Yin, D. Zhao, X. Wang, Y. Ren, L. Zhang, X. Wu, S. Nie, Q. Li, Bio-compatible poly(ester-urethane)s

406   based on PEG-PCL-PLLA copolymer with tunable crystallization and bio-degradation properties, RSC

407   Advances 5(96) (2015) 79070-79080.

408   [37] K. Chrissopoulou, K.S. Andrikopoulos, S. Fotiadou, S. Bollas, C. Karageorgaki, D. Christofilos, G.A.

409   Voyiatzis, S.H. Anastasiadis, Crystallinity and Chain Conformation in PEO/Layered Silicate Nanocomposites,

410   Macromolecules 44(24) (2011) 9710-9722.

411   [38] X. Chen, H. Gao, G. Hai, D. Jia, L. Xing, S. Chen, P. Cheng, M. Han, W. Dong, G. Wang, Carbon nanotube

412   bundles assembled flexible hierarchical framework based phase change material composites for thermal energy

413   harvesting and thermotherapy, Energy Storage Materials 26 (2020) 129-137.

414   [39] P. Roura, J. Farjas, Analytical solution for the Kissinger equation, Journal of Materials Research 24(10)

415   (2009) 3095-3098.

416   [40] X. Zhang, H. Liu, Z. Huang, Z. Yin, R. Wen, X. Min, Y. Huang, Y. Liu, M. Fang, X. Wu, Preparation and

417   characterization of the properties of polyethylene glycol @ Si3N4 nanowires as phase-change materials,

418   Chemical Engineering Journal 301 (2016) 229-237.

419   [41] J. Li, Y. Li, Y. Song, S. Niu, N. Li, Ultrasonic-assisted synthesis of polyvinyl alcohol/phytic acid polymer

420   film and its thermal stability, mechanical properties and surface resistivity, Ultrasonics Sonochemistry 39 (2017)

421   853-862.

422   [42] R.S. Kappes, T. Urbainczyk, U. Artz, T. Textor, J.S. Gutmann, Flame retardants based on amino silanes and

423   phenylphosphonic acid, Polymer Degradation and Stability 129 (2016) 168-179.

424   [43] S. Hao, W. Zhu, H. Huang, M. Yang, J. Zhang, A Phosphorous-Aluminium-Nitride Synergistic Flame

425   Retardant to Enhance Durability and Flame Retardancy of Cotton, ChemistrySelect 4(47) (2019) 13952-13958.

426   [44] P. Zhu, S. Sui, B. Wang, K. Sun, G. Sun, A study of pyrolysis and pyrolysis products of flame-retardant

427   cotton fabrics by DSC, TGA, and PY–GC–MS, Journal of Analytical and Applied Pyrolysis 71(2) (2004) 645-

428   655.

429   [45] M. Wang, G.-Z. Yin, Y. Yang, W. Fu, J.L. Díaz Palencia, J. Zhao, N. Wang, Y. Jiang, D.-Y. Wang, Bio-based

430   flame retardants to polymers: A review, Advanced Industrial and Engineering Polymer Research   (2022).

431   [46] G.-Z. Yin, D.-Y. Wang, Reversible 1:1 Inclusion Complexes of C60 Derivatives in α- and β-Cyclodextrins:

432   Implications for Molecular Recognition-Based Sensing and Supramolecular Assembly, ACS Applied Nano

433   Materials 5(1) (2022) 149-159.

434   [47] J. Jeon, J.H. Park, S. Wi, S. Yang, Y.S. Ok, S. Kim, Latent heat storage biocomposites of phase change

435   material-biochar as feasible eco-friendly building materials, Environmental Research 172 (2019) 637-648.

436   [48] J. Yoo, S.J. Chang, S. Wi, S. Kim, Spent coffee grounds as supporting materials to produce bio-composite

437   PCM with natural waxes, Chemosphere 235 (2019) 626-635.

438   [49] D.G. Atinafu, S. Jin Chang, K.-H. Kim, S. Kim, Tuning surface functionality of standard biochars and the

439   resulting uplift capacity of loading/energy storage for organic phase change materials, Chemical Engineering

440   Journal 394 (2020) 125049.

441   [50] P. Zhang, L. Song, H. Lu, J. Wang, Y. Hu, The influence of expanded graphite on thermal properties for

442   paraffin/high density polyethylene/chlorinated paraffin/antimony trioxide as a flame retardant phase change

443   material, Energy Conversion and Management 51(12) (2010) 2733-2737.

444

Phytic acid as a bio-based flame retardant for Polyrotaxane-based phase change materials

Guang-Zhong Yin, [a, b] Xiao-Mei Yang, [a,] José Luis Díaz Palencia,[b] Jose Hobson, [a] Alba Marta López, [a] De-Yi Wang [a, b,]*

a IMDEA Materials Institute, C/Eric Kandel, 2, 28906 Getafe, Madrid, Spain

b Universidad Francisco de Vitoria, Ctra. Pozuelo-Majadahonda Km 1, 800, 28223, Pozuelo de Alarcón, Madrid, Spain

Corresponding Author

*Tel: +34 91 549 34 22, fax: +34 91 550 30 47; Email: deyi.wang@imdea.org
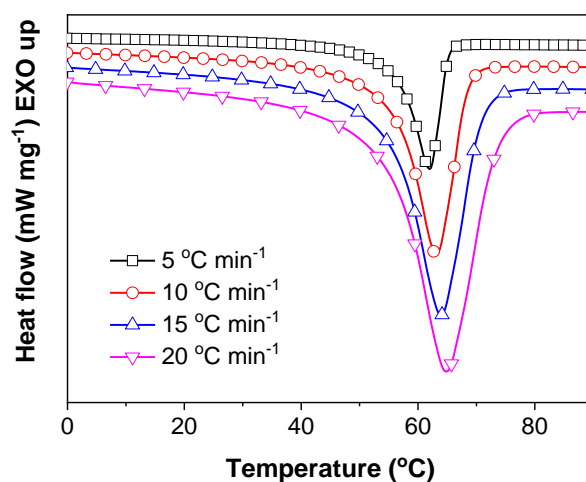
Figure S1. DSC curves of PLR-PA20: melting behavior with different heating rate. (Generally, the samples were run according to the following process for the crystallinity and activation energy (ΔEa): 1: Ramp 20.00 °C min^{-1} to -60.00 °C; 2: Ramp 10.00 °C min^{-1} to 100.00 °C; 3: Ramp 10.00 °C min^{-1} to -60.00 °C; 4: Ramp 10.00 °C min^{-1} to 100.00 °C; 5: Ramp 20.00 °C min^{-1} to -20.00 °C; 6: Ramp 5.00 °C min^{-1} to 100.00 °C; 7: Ramp 20.00 °C min^{-1} to -20.00 °C; 8: Ramp 2.00 °C min^{-1} to 100.00 °C; 9: Ramp 20.00 °C min^{-1} to -20.00 °C; 10: Ramp 20.00 °C min^{-1} to 100.00 °C.)
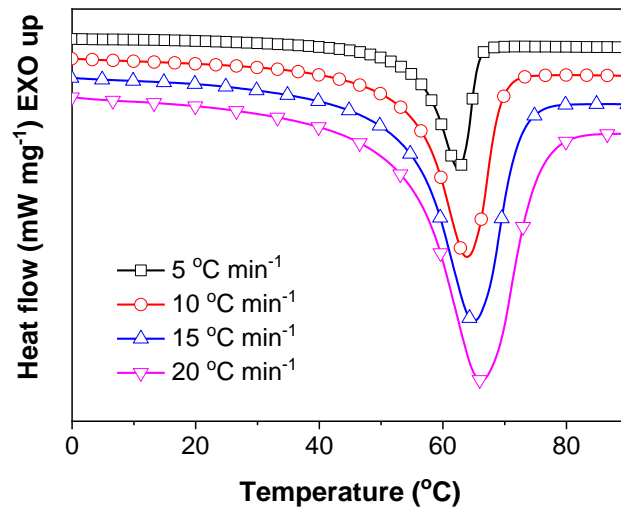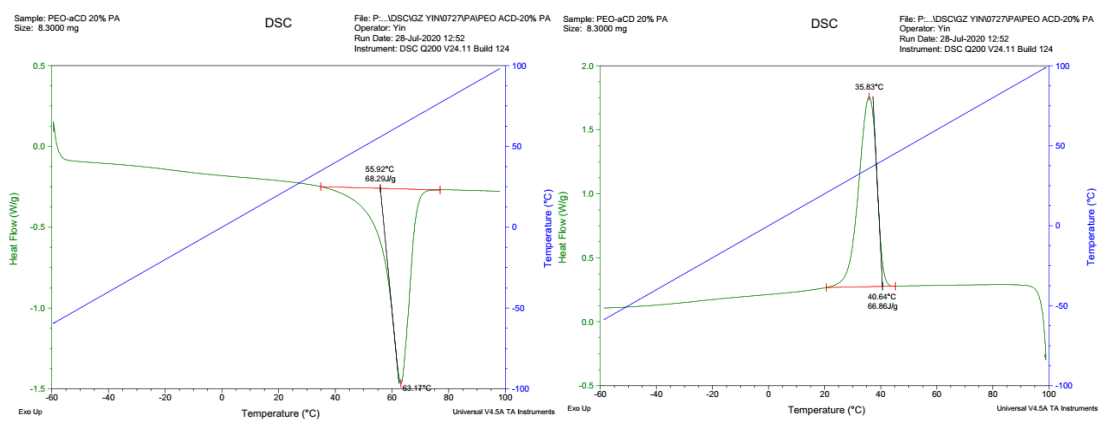
Figure S2. DSC curves of PLR-PA30: melting behavior with different heating rate
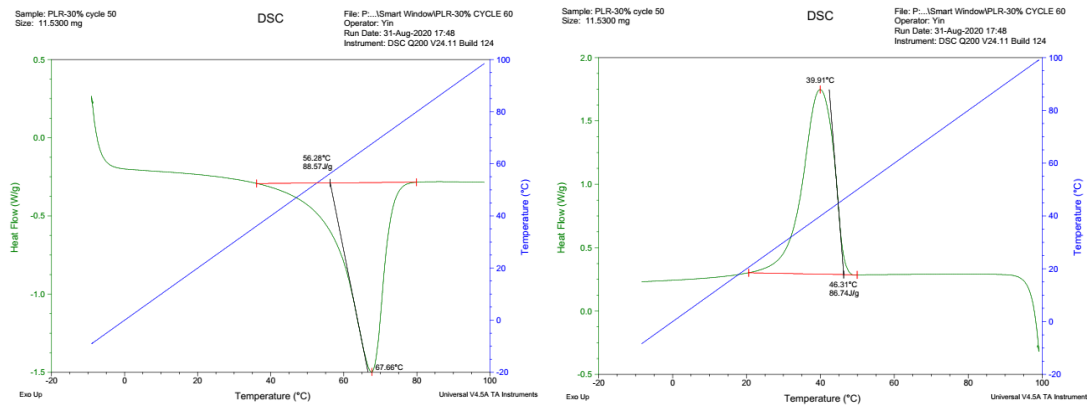
Figure S3. DSC curves of PLR during heating and cooling
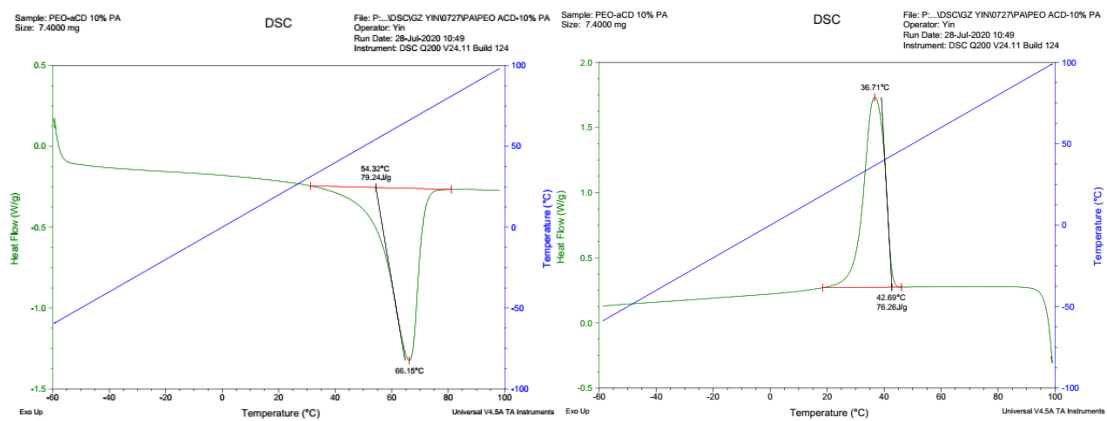
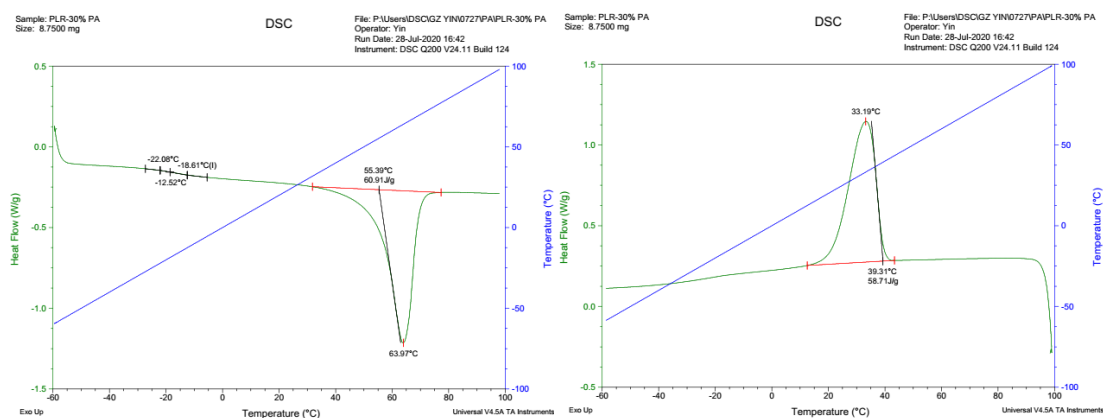**Figure S4**. DSC curves of PLR-PA10 during heating and cooling

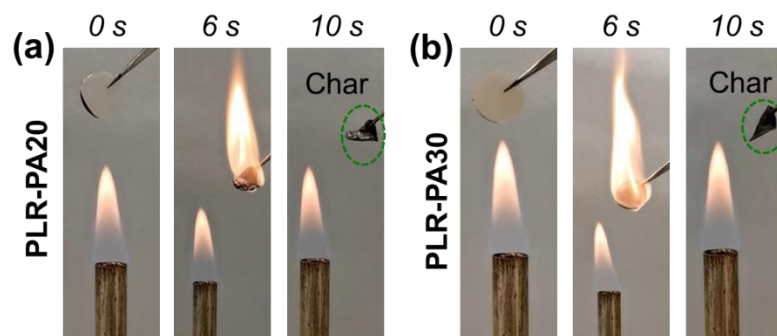**Figure S5**. DSC curves of PLR-PA20 during heating and cooling

Figure S6. DSC curves of PLR-PA30 during heating and cooling

Figure S7. Combustion process of sample (a) PLR-PA20, (b) sample PLR-PA30

Table S1. DSC data list of PEO and the PLRs.

Samples	$T_{m, onset}$ (^{o}C)	$T_{m, peak}$ (^{o}C)	$T_{s, onset}$ (^{o}C)	$T_{s, peak}$ (^{o}C)	ΔH_m (J g^{-1})	ΔH_s (J g^{-1})	Crystallinity (%)
PLR	56.3	67.7	46.3	39.9	88.6	86.7	57.4
PLR-PA10	54.3	66.1	42.7	36.7	79.2	76.3	56.4
PLR-PA20	55.9	63.2	40.6	35.8	68.3	67.9	52.2

26

| PLR-PA30 | 55.1 | 63.9 | 39.3 | 33.2 | 60.9 | 58.7 | 49.6 |

Note: the data were collected based on the curves with heating or cooling rata at 10 ºC min^{-1}.

Table S2. Mechanical properties of the PLRs. Thickness of all the sample is 0.1 mm.

Samples	Young's Modulus (MPa)	Tensile Strength (MPa)	Elongation at break (%)	Yielding strength (MPa)
PLR	826.7±27.5	14.2±0.2	670±57	14.2±0.2
PLR-PA10	1527.4±120.4	24.0±2.6	782±43	22.1±0.5
PLR-PA20	879.5±123.4	21.3±0.3	1115±30	14.2±0.7
PLR-PA30	509.3±31.8	16.0±0.2	1155±12	8.8±0.4

Table S3. The $T_{m, peak}$ of PLR-PAs obtained under different heating rate

Samples	5 ºC min^{-1}	10 ºC min^{-1}	15 ºC min^{-1}	20 ºC min^{-1}
PLR-PA10	63.92	66.15	67.81	69.63
PLR-PA20	61.98	63.17	63.88	64.74
PLR-PA30	62.48	63.97	65.05	66.29

Table S4. Shape memory test results

Samples	Cycle Number	R_f (%)	R_r (%)
PLR	Cycle 1 (C1)	99.31	97.61
-	Cycle 2	99.33	99.80
-	Cycle 3	99.33	99.67
PLR-PA10	Cycle 1	99.54	94.20
	Cycle 2	98.82	99.83
	Cycle 3	99.29	96.13
PLR-PA20	Cycle 1	97.97	95.63
-	Cycle 2	99.62	96.92
-	Cycle 3	99.47	97.01
PLR-PA30	Cycle 1	98.17	95.23
-	Cycle 2	98.71	97.98
-	Cycle 3	98.87	99.86

Table S5. TGA (Air) data list

Samples	$T_{max, 1}$ (ºC)	$T_{max, 2}$ (ºC)	Re. (%, at 600 ºC)
PLR	264.5	332.1	1.1
PLR-PA10	187.7	330.7	5.6
PLR-PA20	172.8	292.4	10.2
PLR-PA30	169.7	281.9	13.6